

## Brain morphometry using 3D moment invariants

J.-F. Mangin<sup>a,b,c,\*</sup>, F. Poupon<sup>a,c</sup>, E. Duchesnay<sup>a,c</sup>, D. Rivière<sup>a,c,d</sup>, A. Cachia<sup>a,b,c</sup>,  
D.L. Collins<sup>e</sup>, A.C. Evans<sup>e</sup>, J. Régis<sup>f</sup>

<sup>a</sup> Service Hospitalier Frédéric Joliot, CEA, 4 place du Général Leclerc, 91401 Orsay Cedex, France

<sup>b</sup> INSERM ERM205, Orsay, France

<sup>c</sup> Institut Fédératif de Recherche 49, Paris, France

<sup>d</sup> INSERM U562, Orsay, France

<sup>e</sup> Montreal Neurological Institute, McGill University, Montreal, Canada

<sup>f</sup> Service de Neurochirurgie Fonctionnelle et Stéréotaxique, La Timone, Marseille, France

Available online 4 August 2004

### Abstract

This paper advocates the use of shape descriptors based on moments of 3D coordinates for morphometry of the cortical sulci. These descriptors, which have been introduced more than a decade ago, are invariant relatively to rotations, translations and scale and can be computed for any topology. A rapid insight into the derivation of these invariants is proposed first. Then, their potential to characterize shapes is shown from a principal component analysis of the 12 first invariants computed for 12 different deep brain structures manually drawn for 7 different brains. Finally, these invariants are used to find some correlates of handedness and sex among the shapes of 116 different cortical sulci automatically identified in each of 142 brains of the ICBM database.

© 2004 Elsevier B.V. All rights reserved.

**Keywords:** Brain; Morphometry; Shape descriptors; Cortical sulci; MRI; Invariant; Handedness

### 1. Introduction

This paper advocates the use of shape descriptors based on moments of 3D coordinates for morphometry purpose. A shorter version has been presented in MIC-CAI'2003 (Mangin et al., 2003a). These 3D descriptors, which are invariant relatively to rotation, symmetry and scale, have been introduced more than a decade ago (Lo and Don, 1989), as a 3D extension to the 2D moment invariants widely used in pattern recognition (Hu, 1962). These 3D moment invariants have not gained a lot of attention in the medical imaging community. In our opinion, however, they provide a

powerful way to perform global morphometry of anatomical entities because they impose no constraint on the object's topology. Therefore, they appear as an interesting alternative to the approaches based on 2D parameterization of the object's surface (Brechtbüler et al., 1995; Gerig et al., 2001; Davies et al., 2002) or of the object's skeleton (Le Goualher et al., 2000; Styner et al., 2003). Such 2D parameterizations, indeed, imply a stable topology, which is difficult to achieve when studying cortical sulci. While the theoretical derivation of the invariants from the coordinate moments is complex, they can be computed in a simple and robust way from a binary volume based description of the objects of interest. This simplicity of use makes these invariants good candidates for mining large databases of objects before using more sophisticated shape analysis tools providing locality to the study (Pizer et al., 1999).

\* Corresponding author. Tel.: 33-1-69-86-77-70; fax: 33-1-69-86-77-68.

E-mail address: [mangin@shfj.cea.fr](mailto:mangin@shfj.cea.fr) (J.-F. Mangin).

URL: <http://anatomist.info/>.

In this paper, the interest of the 3D moment invariants is illustrated through the study of the shapes of the cortical sulci of 142 subjects of the ICBM database. A previous study has shown some correlates of handedness on the global size of some of the sulci of the motor and premotor areas (Mangin et al., 2003b, 2004). These correlates are supposed to stem from handedness-related differences in the pressure to increase the local folding induced by discrepancies in the development of the surrounding cortical areas. This first study has shown that sulcus based morphometry is a compelling complement to the usual voxel-based morphometry (VBM). VBM, indeed, could not reveal any significant handedness-related result with the same database (Watkins et al., 2001), although the existence of some correlates could be forecast from previous manual studies. Such disagreement between both morphometry strategies may stem from the loss of statistical power induced by the non perfect gyral matching performed by the affine spatial normalization underlying this VBM study. While using better spatial normalization strategies may improve the VBM behavior, the variability of the cortical folding pattern seems to prevent a perfect gyral matching. Therefore, sulcus based morphometry may become a new probe to test the assumption that certain neuroanatomical structures may be preferentially modified by particular cognitive skills or diseases.

The first study mentioned above was relying on the size of the pieces of skeleton used to represent the sulci of interest (Mangin et al., 1995). This measure of size is analogous to the volume calculation used in standard morphometric studies. It is evident that sulcus characterization by size does only capture one of the multiple aspects of the folding patterns (Gerig et al., 2001). We propose the use of 3D moment invariants as a richer description of the sulcus shapes. They appear especially adapted to sulcus morphometry, because the numerous and variable sulcus interruptions prevent a simple parameterization strategy for most of the sulci. The next section provides an insight into the origin of the invariants, and a few experiments about their invariance properties and their slow variations in the shape space. The second section reports some invariant-based results relative to the handedness-correlate and sex-correlate study of about 116 sulci automatically labeled in each of 142 brains by a system described elsewhere (Rivière et al., 2002). The last section provides a short discussion about these results.

## 2. 3D moment invariants

In this section, we give a brief insight into the computation of the 3D moment invariants. This insight is not supposed to include all the information required to de-

velop an actual computation software. The aim is to provide an understanding of the origin of the invariance properties of these shape descriptors. A complete description of the theoretical background may be found elsewhere (Lo and Don, 1989; Poupon, 1999). A commandline computing these invariants from a binary image can be found in the brainVISA package (<http://brainvisa.info>).

The 3D moments of order  $n = p + q + r$ ,  $n \in \mathbb{N}$  of a 3D density function  $\rho(x, y, z)$  are defined by

$$m_{pqr} = \int_{-\infty}^{+\infty} \int_{-\infty}^{+\infty} \int_{-\infty}^{+\infty} x^p y^q z^r \rho(x, y, z) dx dy dz. \quad (1)$$

In the following,  $\rho(x, y, z) = 1$ , because we deal with objects defined by binary images. The moments of order higher than 3 will not be considered in this paper for the sake of simplicity, but the derivation of moment invariants is theoretically possible for any order. By discarding moments of order higher than 3, we get a small set of global descriptors which should embed simple shape information like bending, tapering, pinching, etc. The derivation of the invariants aims at filtering out the influence of localization, orientation and scale on the 3D moments in order to obtain “pure shape” descriptors. Translation invariance is simply obtained using central moments. In the following, for the sake of clarity, the origin of the coordinate system is assumed to be at the centroid of the object and the corresponding central moments will be written  $M_{pqr}$ . As shown in (Hu, 1962) for the 2D case, the similitude invariance is obtained by normalizing moments with the suitable power of the volume  $M_{000}$ . Therefore, in the following we consider

$$\mu_{pqr} = \frac{M_{pqr}}{M_{000}^{\frac{p+q+r}{3}+1}}. \quad (2)$$

### 2.1. Rotation invariance

Rotation invariants can be derived from group theory techniques usual in quantum mechanics (Edmonds, 1960). When a rotation is applied to the underlying object, central moments of order  $n$  are transformed into linear combinations of moments of the same order. This result stems from the fact that homogeneous polynomials of order  $n$  form a subspace  $\mathcal{P}_n$  of the functions of  $\mathfrak{R}^3$  stable under the rotation group. The coefficients of the linear combinations mentioned above are the matrix elements of a representation of the 3D rotation group (corresponding to a group homomorphism) (Edmonds, 1960). This representation is reducible, which means that  $\mathcal{P}_n$  can be decomposed into a direct sum of smaller subspaces stable under the rotation group. Rotation invariants stem from the finest possible decomposition leading to irreducible representations. In this new basis,

the effect of the rotation operator on a vector of  $\mathcal{P}_n$  corresponds to a block diagonal matrix

$$D = \begin{pmatrix} D_0 & & & \\ & (D_1) & & \\ & & \ddots & \\ & & & (D_L) \end{pmatrix}, \quad (3)$$

where  $D_0, \dots, D_L$  are irreducible representations (Edmonds, 1960).

The basis corresponding to this decomposition is the basis of harmonic polynomials  $y_l^m = r^l Y_l^m$ ,  $l=0, \dots, L$ ,  $m=-l, \dots, l$ , where  $Y_l^m$  are the spherical harmonics and  $r = \sqrt{x^2 + y^2 + z^2}$ . In the following,  $\mathcal{E}_l$  denotes the subspace defined by harmonic polynomials of order  $l$ . The space  $\mathcal{P}_n$  of homogeneous polynomials of order  $n$  decomposes itself into subspaces  $\mathcal{E}_n, \mathcal{E}_{n-2}, \mathcal{E}_{n-4}$ , etc. For instance  $\mathcal{P}_2$  splits into  $\mathcal{E}_2$  and  $\mathcal{E}_0$ ,  $\mathcal{P}_3$  splits into  $\mathcal{E}_3$  and  $\mathcal{E}_1$ , etc. In the new basis of  $\mathcal{P}_n$ , moments  $\mu_{pqr}$  are transformed into complex moments  $v_l^m$  and rotation invariants are derived from  $v_l^m$  using tensor products, which may be understood as a generalization of scalar or vector products (Lo and Don, 1989; Edmonds, 1960).

If  $\{e_i\}$  is the basis of a vector space  $\mathcal{V}$ , then any vector  $x$  of  $\mathcal{V}$  may be represented as

$$x = \sum_i x^i e_i = x^i e_i, \quad (4)$$

where the Einstein summation convention has been assumed in the rightmost expression. A new basis  $\{\tilde{e}_i\}$  is related to the original basis by

$$\tilde{e}_i = A_i^j e_j \quad \text{or} \quad e_i = a_i^j \tilde{e}_j, \quad (5)$$

where  $A_i^j$  denotes a linear transformation, and  $a_i^j$  its inverse. Any form  $T_{l_1 \dots l_p}^{m_1 \dots m_q}$  is said to be a tensor of covariant rank  $p$  and contravariant rank  $q$  if it transforms itself according to the equation

$$\tilde{T}_{k_1 \dots k_p}^{n_1 \dots n_q} = A_{k_1}^{l_1} \dots A_{k_p}^{l_p} a_{m_1}^{n_1} \dots a_{m_q}^{n_q} T_{l_1 \dots l_p}^{m_1 \dots m_q}. \quad (6)$$

Particularly, scalars are rank-0 tensors and vectors are rank-1 tensors. In the following, only rank-0 and rank-1 tensors will be considered. For instance the  $v_l^m$  are rank-1 contravariant tensors of the space  $\mathcal{E}_l$ . It must be pointed out that only  $m$  is a tensor index. Rotation invariants are rank-0 tensors of  $\mathcal{E}_0$ . They are constructed using tensor product according to the following formula (Edmonds, 1960): let  $T_l^m$  denote a tensor of  $\mathcal{E}_l$ , then  $\forall T_{l_1}^{m_1}, T_{l_2}^{m_2}$ , a new tensor of  $\mathcal{E}_l$  is produced by

$$T_l^m = \sum_{m_1, m_2} \langle l_1, m_1, l_2, m_2 \mid l_1, l_2, l, m \rangle T_{l_1}^{m_1} T_{l_2}^{m_2}, \quad (7)$$

$$|l_1 - l_2| \leq l \leq l_1 + l_2,$$

where  $\langle l_1, m_1, l_2, m_2 \mid l_1, l_2, l, m \rangle$  is the vector coupling or Clebsch–Gordan coefficients, which are computed using recursive formula (Edmonds, 1960).

An intuitive understanding of the tensor product described by formula (7) can be given by the following considerations:

- (1) if  $l_1 = l_2$  and  $l = 0$ ,  $T_0^m$  is related to a scalar product;
- (2) if  $l \neq 0$ ,  $T_l^m$  is related to a vector cross product.

Rotation invariants are inferred from all the possible applications of the tensor product to  $v_0^m, v_1^m, v_2^m$  and  $v_3^m$  yielding rank-0 tensors, namely scalars which are the 3D moment invariants. These invariants turn out to be homogeneous polynomials of central moments. Because of various symmetries, the tensor products results only in 12 invariants  $I_\beta^\alpha$ , where  $\alpha$  denotes the order of the underlying central moments and  $\beta$  denotes the subspace indices of the different tensors used in the application of the products (Lo and Don, 1989; Poupon et al., 1997). Thus, we get four norms  $I_{00}^2, I_{11}^3, I_{22}^2$  and  $I_{33}^3$ , five scalar products and norms of new tensors  $I_{222}^2, I_{3111}^3, I_{3131}^3, I_{3331}^3$  and  $I_{3333}^3$ , and three last invariants derived by combining the second- and third-order moments  $I_{112}^{2,3}, I_{312}^{2,3}$  and  $I_{332}^{2,3}$ . Since moment invariants are expressed by homogeneous polynomials, they can be finally reduced by the suitable power of the invariant (Burel and Hénoq, 1995). This reduction aims at normalizing the range of variation of each invariant. Then each invariant  $I_\beta^\alpha$  is transformed in

$$\tilde{I}_\beta^\alpha = \text{sign}(I_\beta^\alpha) \cdot |I_\beta^\alpha|^{1/d}, \quad (8)$$

where  $\tilde{I}_\beta^\alpha$  is the reduced moment invariant and  $d$  the polynomial degree.

## 2.2. A few experiments

In order to check that the theoretical properties of invariance stand for discrete representations of objects relying on binary images, two simple shapes have been resampled with 28 different orientations. Each invariant has been computed for each orientation. The obtained standard deviations are almost negligible relatively to the means, which shows that the rotation invariance is respected (see Fig. 1). The standard deviations are higher for the ventricle than for the pinched superquadric, which can be understood from the fact that the resampling induces more modifications of the thinnest shape.

In order to check that the 3D moment invariants vary sufficiently slowly in the shape space to be interesting as shape descriptors, we have performed a simple principal component analysis of the invariants obtained for six different kinds of shapes corresponding to deep brain nuclei and lateral ventricles. These objects have been manually drawn by a neuroanatomist in the two hemispheres of seven different brains and can be visualized in Fig. 2. Plotting the 84 objects in a chart corresponding to the three first axes yielded by the PCA shows that

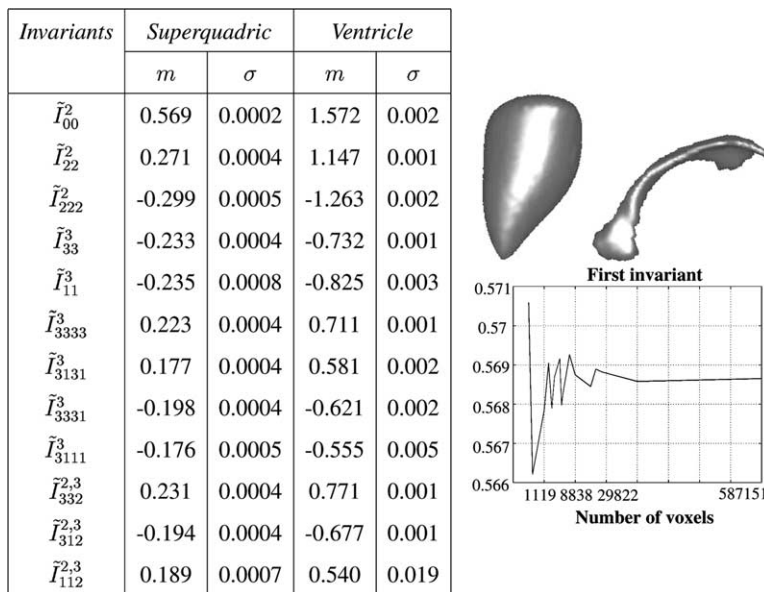


Fig. 1. Left: means and standard deviations of the 12 invariants for 28 different orientations of the two objects visualized in the figure. Right: typical variations observed for different sampling of the pinched superquadric. NB: in all figures, for the sake of visualization, voxel-based objects are triangulated before 3D rendering.

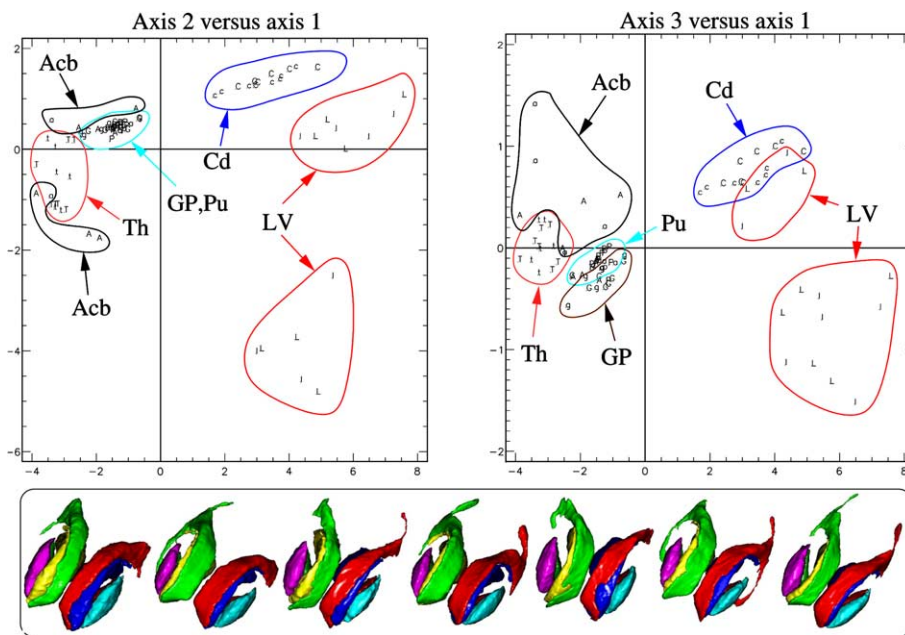


Fig. 2. The 84 deep anatomical objects used to analyze the shape representation provided by the 3D invariants. The 12 invariants have been computed for each nucleus. Then a standard PCA has been performed and each nucleus is plotted in two charts corresponding to the 3 principal axes of the PCA. Abbreviations denote Acb, accumbens; Th, thalamus; Cd, caudate; GP, globus pallidus; Pu, putamen; LV, lateral ventricle. For each point, lower and upper case letters denote left and right hemispheres. (For interpretation of the references to colour in this figure legend, the reader is referred to the web version of this article.)

the instances of each anatomical entity gather in one localized region of the shape space, as described by the invariants. Furthermore, the regions corresponding to two nuclei with similar shapes, are closed in this space. This is for instance clear for the pairs (caudate nucleus,

lateral ventricle), or (putamen, globus pallidus). These properties have been used previously to design shape probability distributions embedded in a Bayesian framework to bias a multi-object deformable model dedicated to brain basal ganglia (Poupon et al., 1998).

### 3. Result

A large scale morphometric study of the handedness and sex correlates has been performed on a sulcus-by-sulcus basis, each sulcus being identified automatically by a computer vision system freely available on <http://anatomist.info>. The subjects scanned were 142 unselected normal volunteers previously used for the VBM studies mentioned above (Watkins et al., 2001); 82 were male and 60 were female. On a short handedness questionnaire, 14 subjects were dominant for left-hand use on a number of tasks; the remaining 128 subjects preferred to use their right hand. The 142 T1-weighted brain volumes were stereotaxically transformed using nine parameters (Collins et al., 1994) to match the Montreal Neurological Institute 305 average template. The cortical folds were then automatically extracted using a 3D skeletonization (Mangin et al., 1995). Finally, 58 cortical sulci were automatically recognized in each hemisphere using only one stochastic optimization (Rivière et al., 2002).

The size of each sulcus was computed as the number of voxels included in its skeletonized representation. It should be noted that this measurement depends on the sulcus orientation because of the discrete sampling. A better estimation of the sulcus surface would be computed for instance from a mesh of this voxel-based representation. In this paper, however, we use this voxel-based measurement because it can be considered as the moment of order 0 of the shape. Remember, anyway, that the first part of the paper has shown that the robustness to sampling phenomena of the invariants is much better than in the case of this volume measurement.

Then, left ( $L$ ) and right ( $R$ ) sizes were used to obtain a normalized asymmetry index  $((L-R)/(L+R)/2)$  for each sulcus and each brain. For each sulcus, standard  $t$ -tests were used to compare the distribution of sizes and asymmetry indices either between left-handed and right-handed groups, or between male and female groups. Mann–Whitney  $U$  tests were also performed to be more resistant to outliers, leading to qualitatively similar results. Several significant handedness correlates were revealed by our analysis ( $p < 0.05$ , not corrected for multiple comparisons), including most of the sulci of the motor areas: central sulcus ( $p = 0.02$ ), intermediate precentral sulcus ( $p = 0.03$ ) and inferior precentral sulcus ( $p = 0.05$ ) (see Fig. 3).

To test if the 3D invariants can capture additional information about the handedness correlates on the folding patterns, the 12 invariants have been computed for each sulcus and each brain. For this computation, each sulcus instance is represented by a set of voxels of the global skeleton. We observed first that the variance introduced by sampling during the first experiment (cf. Fig. 1) is much lower than the inter-individual var-

iability of the invariants computed for the sulci. For each sulcus, a standard  $t$ -test was used to compare the invariant distributions of left-handed and right-handed groups. It should be noted that this analysis involved  $12 \times 116 = 1392$  tests, which calls for some correction for multiple testing. This correction however requires further work to take into account the complex dependences between these tests. With  $p < 0.001$ , only two sulci yielded significant results: the right inferior post-central sulcus (2 invariants) and the left superior frontal sulcus (7 invariants). These sulci had not yielded significant size asymmetry index differences between both populations (see the size distributions of the frontal sulcus in Fig. 3). Interestingly, with  $p < 0.01$ , none of the sulci presenting significant results with size index led to results for 3D invariants, which tends to prove that these descriptors are really invariant for scale (see the fourth invariant distribution for the right central sulcus in Fig. 3).

One of the difficulties with global shape descriptors like 3D invariants is the lack of simple interpretation in natural language terms. Considering the invariants as a first probe for exploratory analysis, however, such interpretation can be inferred by visual inspection of the extreme instances of both populations. This has been done for the superior frontal sulcus using the invariant ( $I_{33}^2$ ) yielding the most significant result, leading to the fact that the sulcus of the right-handed population is deeper backwards, near the central sulcus, than forwards, in the frontal part (see Fig. 4). This observation may be related to models of the folding process, like the tension-based mechanism introduced by (Van Essen, 1997).

The results of the previous experiment has shown the possibility to compare shapes with different topologies. The superior frontal sulcus, indeed, is often interrupted. To explore further this potential, complex shapes have been built from sets of simpler sulci. We do not claim that this kind of construction process can be performed along an exhaustive strategy. Combinatorial explosion would then lead to various difficulties. A construction approach, however, may have some interest to explore the sulcus patterns according to a priori hypotheses. For instance, looking for handedness correlates around motor related areas is attractive. Therefore, the sulcus surrounding the motor areas which had led to size-related handedness correlates have been merged into four different aggregates (see Fig. 5). The 12 invariants have been computed for each aggregate instance. These invariants have led to significant correlation with handedness for the left motor aggregate made up of central sulcus, inferior and intermediate precentral sulci ( $p = 0.03$ ) (see Fig. 5). Visual inspection of the extreme cases led to observe a specific pattern, namely an intermediate precentral sulcus more parallel to the central sulcus in the right-handed population than in the left-handed population (see Fig. 6).

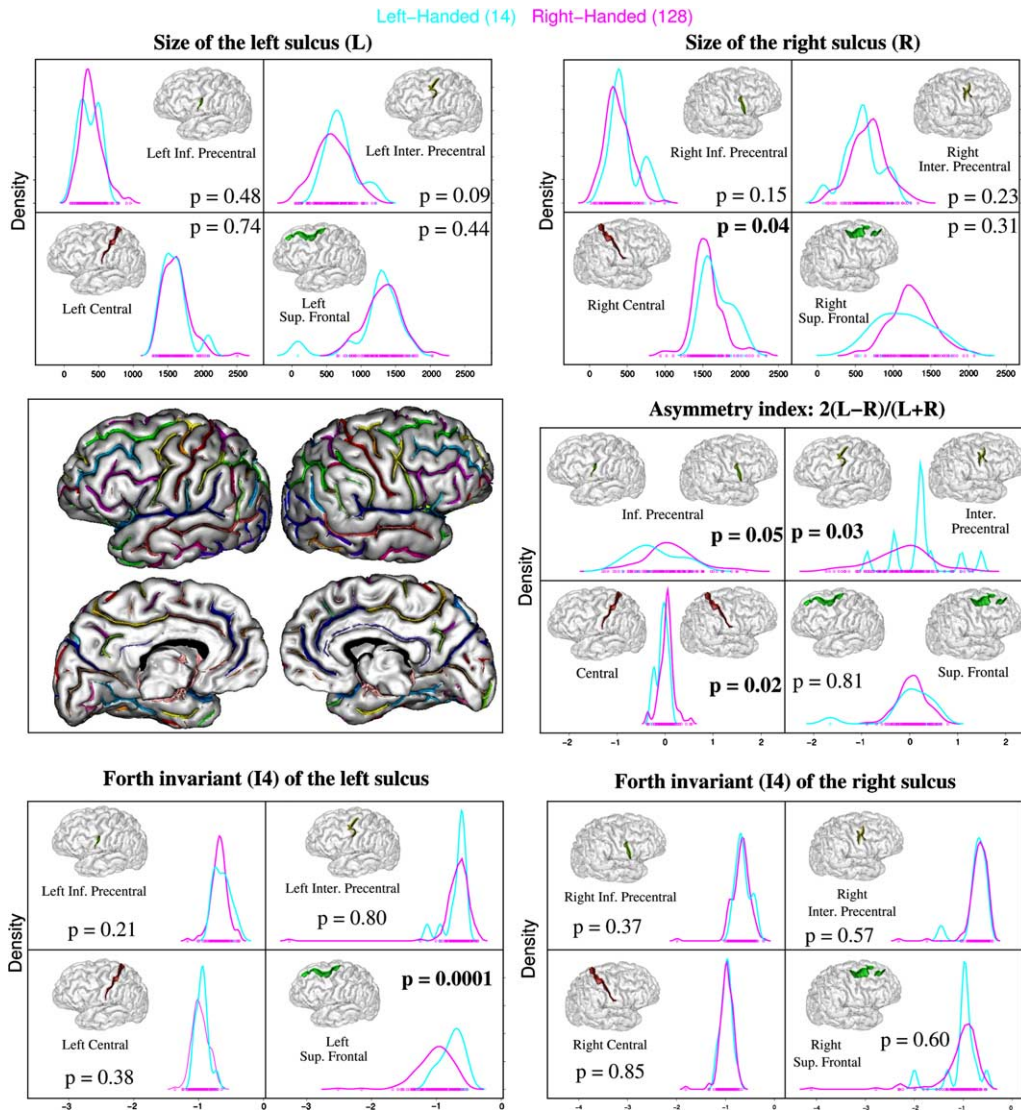


Fig. 3. Middle left: one example of the 142 brains with labeled sulci used for this study. Top: distributions of the sizes of a few sulci for left-handed and right-handed populations. These distributions stem from the Gaussian kernel estimator of R software (Venables and Ripley, 2002). Standard  $t$ -tests show no significant difference between the two populations relatively to these distributions except for the right central sulcus, which houses the primary motor areas controlling the left hand: the average right central sulcus appears bigger for left-handed people. Middle right: the estimated distributions of a simple asymmetry index present significant handedness correlates for three of the sulci surrounding the motor areas (central and precentral sulci). In return no handedness correlate is observed for the superior frontal sulcus. Bottom: the distributions of the fourth invariant ( $I_{33}$ ) for the same sulci. Standard  $t$ -tests show that the distribution related to the left superior frontal sulcus is the only one presenting some correlation with handedness. (For interpretation of the references to colour in this figure legend, the reader is referred to the web version of this article.)

The previous experiments performed on handedness correlates embed a weakness related to the small size of the left-handed population. The small number of sulcus instances stemming from the left-handed population, indeed, limits the possibility to infer some clear understanding of the shape feature leading to different invariant distributions. Therefore, we performed a last experiment on sex correlates on the invariants, which led us to compare 82 males versus 60 females. The sulcus leading to the strongest statistical effect is the right Collateral Fissure (see Fig. 7). No significant sex-related effect was observed for the sulcus size. The distribution of the fourth invariant, however, was significantly corre-

lated with sex ( $p=0.001$ ). Sorting the sulci according to the value of this invariant highlights the fact that the curvature associated to the genus of the S shape of the sulcus is more important for females. Because of this higher curvature, female's sulci have a smaller wingspan in Talairach's frame.

#### 4. Discussion

The results mentioned in this paper show that interesting global shape descriptors can be derived from the moments of coordinates. They do not stand as rivals

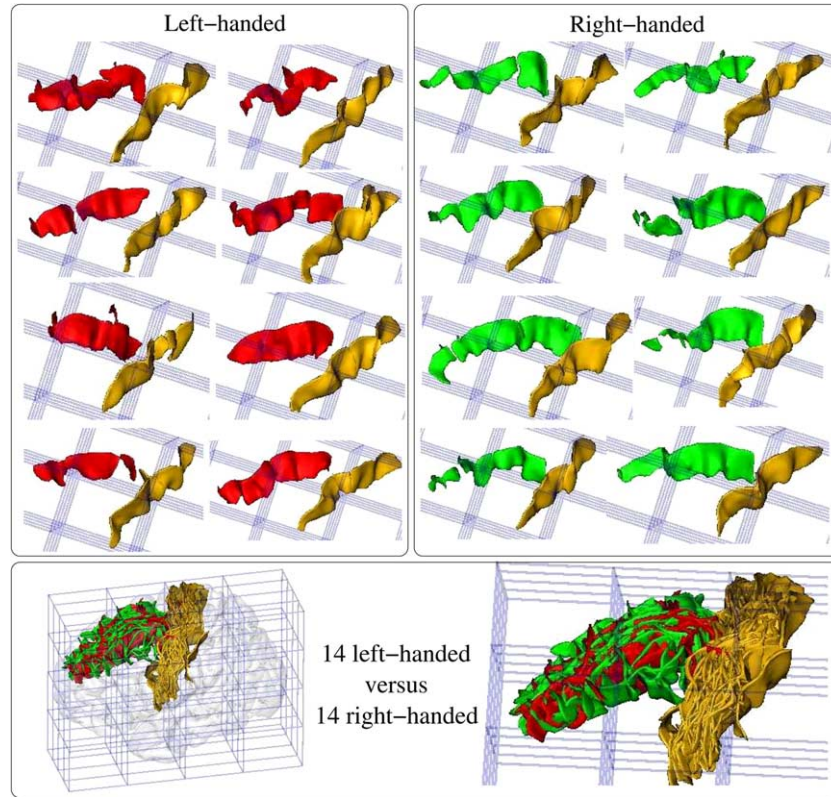


Fig. 4. Top: the 8 left superior frontal sulci (red or green) of both populations leading to the most separate values for the invariant of Fig. 3, namely the 8 highest values for the left-handed subjects and the 8 lowest values for the right-handed subject. The sulci of the right-handed population are deeper near central sulcus (gold) than in the more frontal part. The grid corresponds to Talairach orientation. Bottom: the superior frontal sulci of the 14 left-handed subjects mixed with 14 right-handed subjects matching for age and sex. The sulci are gathered in Talairach system. The variability of the localization of the sulcus in this coordinate system seems globally similar for both populations. (For interpretation of the references to colour in this figure legend, the reader is referred to the web version of this article.)

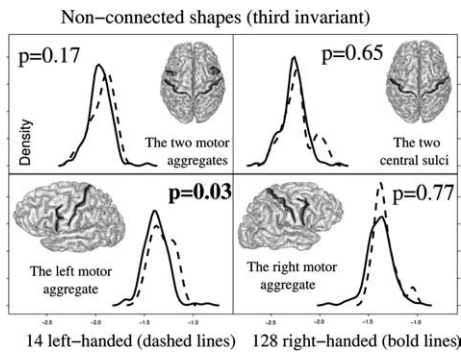


Fig. 5. The distributions of the third invariant ( $I_{22}^2$ ) for complex shapes made up of several sulci bordering the motor areas and showing some handedness correlates on size (see Fig. 3). These shapes include several connected components. The invariant average value is correlated with handedness for the left motor aggregate made up of inferior and intermediate precentral sulci and central sulcus.

for the global descriptors that may stem from the object's surface parameterization strategy (Gerig et al., 2001; Davies et al., 2002) or the object's skeleton (Le Goualher et al., 2000; Styner et al., 2003). They are also complementary to the warping-based strategy widely

used in the brain mapping community (Csernansky et al., 1998; Ashburner and Friston, 2000; Toga and Thompson, 2002; Ashburner et al., 2003; Shen and Davatzikos, 2003). The notion of shape is too rich indeed to be fully described by one point of view. Hence, moment invariants are just one more toolbox to compare shapes, which is especially interesting when the topology varies among the population. It should be noted that a wider set of invariants could be derived, using higher order moments, leading to more description power. However, deriving these higher order moments can be especially complex and may lead to instabilities during computation.

Another simpler way of adding new descriptors based on the same theoretical background consists in computing the moments for a mesh of the object surface, which would lead to another set of invariants. This idea could even be extended to the moments computed for various objects obtained by rotation-invariant transformations, for instance eroded or dilated versions of the initial object. One may argue that other simpler invariants can be derived from the moments using algebraic techniques. While this is true for the moments of order 2 leading

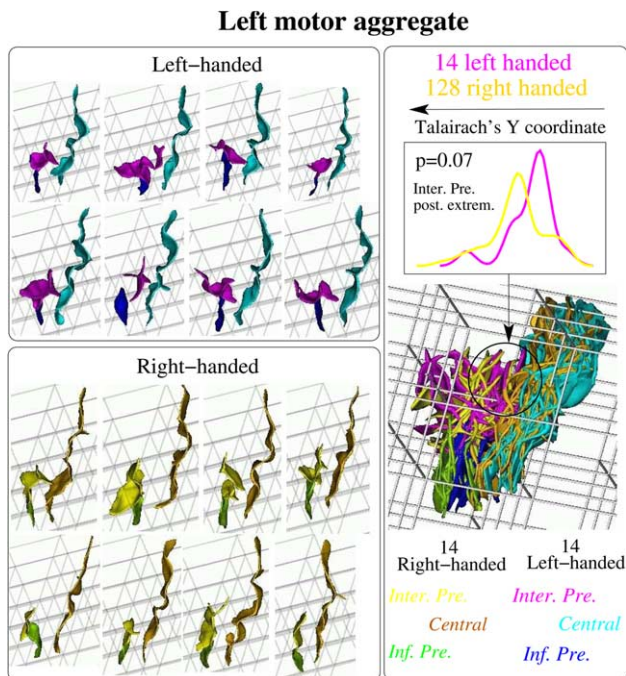


Fig. 6. Left: the 8 subjects of both populations leading to the most separate values for the third invariant computed for the left motor complex (cf. Fig. 5), namely the 8 lowest values for right-handed subjects and the 8 highest values for left-handed subjects. The motor complex is made up of three sulci, which have yielded handedness correlated asymmetry indices (Mangin et al., 2003b) (cf. Fig. 3): central (cyan/gold), intermediate precentral (violet/yellow) and inferior precentral (blue/green) sulci. The intermediate precentral sulcus seems more parallel to the central sulcus in right-handed subjects. Right: the same sulci for the 14 left-handed subjects mixed with 14 right-handed subjects matching for age and sex. Added to the fact that the motor sulci of the left-handed subjects seem shifted toward the back of the brain, the apparent link between handedness and intermediate precentral sulcus orientation leads to differences in the distributions of the  $Y$  coordinate of the posterior extremity of its junction with the brain hull ( $p$ -value stems from a  $t$ -test). (For interpretation of the references to colour in this figure legend, the reader is referred to the web version of this article.)

to inertia moments, it remains unclear if similar invariants can be derived from higher order moments. This is an interesting direction of research, however, because such invariants lead to simpler geometric interpretation.

While the invariance properties are very attractive to deal with shape, they sometimes lead to a loss of description power. In some situations, indeed, two shapes obtained from one another through a  $180^\circ$  rotation should be distinguished, which cannot be done with this set of invariants. Let us imagine a situation where left-handedness would lead to a shallower superior frontal sulcus backwards to be compared to the shallower sulcus forwards for right-handedness (cf. Fig. 4). This imaginary situation would lead to the same invariant distributions for both populations. Therefore, for some applications, the simple coordinate moments computed in a coordinate system of reference like Talairach's pro-

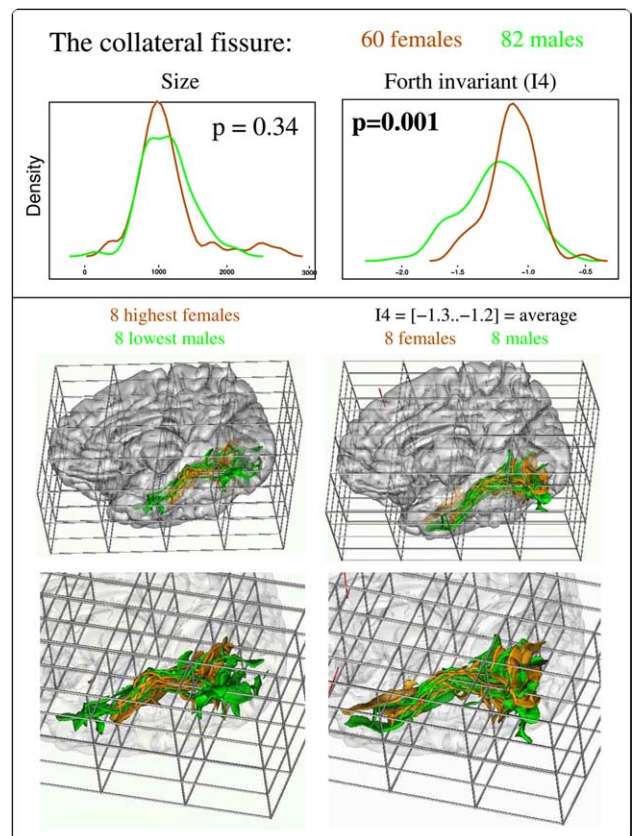


Fig. 7. Top: the sex related distributions of the size and of the fourth invariant ( $I_{33}^2$ ) for the collateral fissure. The average fourth invariant is correlated with sex while the sulcus size is not. Down left: the 8 subjects of both populations leading to the most separate values for the fourth invariant, namely the 8 lowest values for males and the 8 highest values for females. Female's sulci seem to have a smaller wingspan because of higher curvature. Down right: 8 males and 8 females picked in the range of average values for the invariant. (For interpretation of the references to colour in this figure legend, the reader is referred to the web version of this article.)

portional system could be more interesting. Of course, with such an approach, the variability of the object's orientation in the reference system adds some variance to the moments, which could mask some interesting shape features.

One of the key difficulty when using moment invariants is the lack of clear interpretation of the invariant's meaning relatively to the shape. It may be interesting to study the behavior of these invariants for families of synthetic shapes controlled by only a few parameters. However, there is no reason to hope that each invariant describes a simple independent geometric feature. Indeed, some of the invariants are highly correlated. Therefore, we do not even know how many actual degrees of freedoms are covered by the set of 12 invariants used in this paper. This may be addressed through the synthesis of a set of random shapes, but there is no straightforward way to generate an exhaustive set.

In this paper, we have used the moment invariants as probe detecting population-dependent features of the cortical folding patterns. We have used large populations to lower the influence of the errors of our sulcus recognition system, but we cannot discard yet the possibility of some bias induced by the learning database used to train our artificial neuroanatomist (Rivière et al., 2002). It should be noted that the invariants could be added in a near future to the set of shape descriptors used by our pattern recognition system.

It is interesting to discuss why subtle variations of the sulcus shapes may be correlated with cognitive or genetic features. This idea stems from hypotheses about the various forces driving the folding process during brain growth (Régis et al., 1995; Van Essen, 1997). These forces are supposed to include the expansion of the different cortical areas and the tensions induced by the underlying fiber bundles. In some genetic diseases, this folding process is deeply modified, which may stem directly from modifications of the brain architecture (Molko et al., 2003). Smaller modifications of the sulcal shapes could also occur because of the development of the local neural circuitry induced by specialized or preferred behavior (Draganski et al., 2004). Such development may not only increase the cortical thickness but also modify the balance between the various tensions sculpting the folding patterns. Hence, an increased expansion of one given architectonic area could lead to a deformation of the surrounding sulcal pattern. An increased tension from one long range fiber bundle could also modify the folding patterns.

As an illustration of this point of view, the size asymmetry of the central sulcus and of the inferior precentral sulci could be easily related to an increase of the surface of the motor gyrus in the hemisphere contralateral to handedness (White et al., 1994; Amunts et al., 1996). In return, the intermediate precentral sulcus which is folded orthogonally to the motor gyrus is less developed in the most active hemisphere. The second experiment in this paper has even shown that this orthogonal sulcus becomes often parallel to the central sulcus in the dominant hemisphere. Both observations could be induced by the expansion of the motor gyrus or by differences in the development of the motor gyrus connectivity. The new opportunities provided by diffusion imaging should lead to new insight about the role of connectivity. Recent results, for instance, have shown increased anisotropy in the white matter underlying the dominant motor gyrus (Buchel et al., 2004) or more extensive connectivity of the motor system in the dominant hemisphere (Guye et al., 2003). While it is too soon to untangle the links between all these phenomena, we hope that a better understanding may stem one day from a model of the various forces acting on the folding process in the precentral area.

## 5. Conclusion

The descriptors used in this paper will be used in a near future to study the influence of cognitive, genetic or pathologic features on the shapes of various other cerebral objects like gyri (Cachia et al., 2003), deep nuclei (Poupon et al., 1998) or fiber bundles (Poupon et al., 2000; Mangin et al., 2002). In order to improve such studies, we will have to develop a better understanding of the domain of shape space where the invariants have a good discriminatory power. More complex aggregates made up of several anatomical objects could also be studied following specific neuroscience hypotheses. Finally, the moment invariants computed for these various anatomical structures will be mixed with other shape descriptors to develop population classification algorithms (Duchesnay et al., 2004). Such algorithms gathering the discriminatory power of various anatomical features may provide soon new powerful diagnostic tool.

## References

- Amunts, K., Schlaug, G., Schleicher, A., Steinmetz, H., Dabringhaus, A., Roland, P.E., Zilles, K., 1996. Asymmetry in the human motor cortex and handedness. *NeuroImage* 4, 216–222.
- Ashburner, J., Friston, K.J., 2000. Voxel-based morphometry – the methods. *NeuroImage* 11, 805–821.
- Ashburner, J., Csernansky, J.G., Davatzikos, C., Fox, N.C., Frisoni, G.B., Thompson, P.M., 2003. Computer-assisted imaging to assess brain structure in healthy and diseased brains. *The Lancet Neurology*, 2.
- Brechtbüler, C., Gerig, G., Kübler, O., 1995. Parametrization of closed surfaces for 3D shape description. *Computer Vision and Image Understanding* 61 (2), 154–170.
- Buchel, C., Raedler, T., Sommer, M., Sach, M., Weiller, C., Koch, M.A., 2004. White matter asymmetry in the human brain: a diffusion tensor mri study. *Cerebral Cortex*, 2004 (in press).
- Burel, G., Hénoq, H., 1995. Three-dimensional invariants and their application to object recognition. *Signal Processing* 45 (1), 1–22.
- Cachia, A., Mangin, J.-F., Rivière, D., Papadopoulos-Orfanos, D., Kherif, F., Bloch, I., Régis, J., 2003. A generic framework for parcellation of the cortical surface into gyri using geodesic Voronoi diagrams. *Medical Image Analysis* 7 (4), 403–416.
- Collins, D.L., Neelin, P., Peters, T.M., Evans, A.C., 1994. Automatic 3D intersubject registration of MR volumetric data in standardized talairach space. *Journal of Computer Assisted Tomography* 18 (2), 192–205.
- Csernansky, J., Joshi, S., Wang, L., Haller, J., Gado, M., Miller, J., Grenander, U., Miller, M., 1998. Hippocampal morphometry in schizophrenia via high dimensional brain mapping. *Proceedings of the National Academy of Sciences of the USA* 95, 11406–11411.
- Davies, R.H., Twining, C., Cootes, T.F., Taylor, C.J., 2002. A minimum description length approach to statistical shape modelling. *IEEE Transactions on Medical Imaging* 21, 525–537.
- Draganski, B., Gaser, C., Busch, V., Schuierer, G., Bogdahn, U., May, A., 2004. Neuroplasticity: Changes in grey matter induced by training. *Nature* 427, 311–312.
- Duchesnay, E., Roche, A., Rivière, D., Papadopoulos-Orfanos, D., Cointepas, Y., Mangin, J.-F., 2004. Population classification based on structural morphometry of cortical sulci. In: *2nd Proceedings of the IEEE ISBI*, Arlington, VA, pp. 1276–1279.

- Edmonds, A.R., 1960. *Angular Momentum in Quantum Mechanics*. Princeton University Press, New Jersey.
- Gerig, G., Styner, M., Shenton, M.E., Lieberman, J.A., 2001. Shape versus size: Improved understanding of the morphology of brain structures. In: *MICCAI 2001, Lecturer Notes on Computer Science*, vol. 2208. Springer, Berlin, pp. 24–32.
- Guye, M., Parker, G.J., Symms, M., Boulby, P., Wheeler-Kingshott, C.A., Salek-Haddadi, A., Barker, G.J., Duncan, J.S., 2003. Combined functional mri and tractography to demonstrate the connectivity of the human primary motor cortex in vivo. *Neuroimage* 19 (4), 1349–1360.
- Hu, M.-K., 1962. Visual pattern recognition by moment invariants. *IRE Transactions on Information Theory* 8 (February), 179–187.
- Le Goualher, G., Argenti, A.M., Duyme, M., Baare, W.F., Hulshoff-pol, H.E., Boomsma, D.I., Zouaoui, A., Barillot, C., Evans, A.C., 2000. Statistical sulcal shape comparisons: application to the detection of genetic encoding of the central sulcus shape. *Neuroimage* 11 (5), 564–574.
- Lo, C.-H., Don, H.-S., 1989. 3D moment forms: their construction and application to object identification and positioning. *IEEE PAMI* 11 (October), 1053–1064.
- Mangin, J.-F., Frouin, V., Bloch, I., Régis, J., López-Krahe, J., 1995. From 3D magnetic resonance images to structural representations of the cortex topography using topology preserving deformations. *Journal of Mathematical Imaging and Vision* 5 (4), 297–318.
- Mangin, J.-F., Poupon, C., Cointepas, Y., Rivière, D., Papadopoulos-Orfanos, D., Clark, C.A., Régis, J., Le Bihan, D., 2002. A framework based on spin glass models for the inference of anatomical connectivity from diffusion-weighted MR data. *NMR in Biomedicine* 15, 481–492.
- Mangin, J.-F., Poupon, F., Rivière, D., Collins, D.L., Evans, A.C., Régis, J., 2003a. 3D Moment Invariant Based Morphometry. In: Peters, T., Elli, R. (Eds.), *MICCAI, Montreal, Lecturer Notes on Computer Science*, vol. 2879. Springer, Berlin, pp. 505–512.
- Mangin, J.-F., Rivière, D., Cachia, A., Papadopoulos-Orfanos, D., Collins, D.L., Evans, A.C., Régis, J., 2003b. Object-based strategy for morphometry of the cerebral cortex. In: *IPMI, Ambleside, UK, Lecturer Notes on Computer Science*, vol. 2732. Springer, Berlin, pp. 160–171.
- Mangin, J.-F., Rivière, D., Cachia, A., Duchesnay, E., Cointepas, Y., Papadopoulos-Orfanos, D., Collins, D.L., Evans, A.C., Régis, J., 2004. Object-based morphometry of the cerebral cortex. *IEEE Transactions On Medical Imaging*, 2004 (in press).
- Molko, N., Cachia, A., Rivière, D., Mangin, J.-F., Bruandet, M., Le Bihan, D., Cohen, L., Dehaene, S., 2003. Functional and structural alterations of the intraparietal sulcus in a developmental dyscalculia of genetic origin. *Neuron* 40 (4), 847–858.
- Pizer, S.M., Fritsch, D.S., Yushkevich, P.A., Johnson, V.E., Chaney, E.L., 1999. Segmentation, registration, and measurement of shape variation via image object shape. *IEEE Transactions on Medical Imaging* 18 (10), 851–865.
- Poupon, C., Clark, C.A., Frouin, V., Régis, J., Bloch, I., LeBihan, D., Mangin, J.-F., 2000. Regularization of diffusion-based direction maps for the tracking of brain white matter fascicles. *NeuroImage* 12 (2), 184–195.
- Poupon, F., 1999. *Parcellisation systématique du cerveau en volumes d'intérêt. Le cas des structures profondes*. Ph.D. Thesis. Available from <http://brainvisa.info>, INSA Lyon, Lyon, France.
- Poupon, F., Mangin, J.-F., Frouin, V., Magnin, I., 1997. 3D multi-object deformable templates based on moment invariants. In: *10th SCIA*, vol. I, pp. 149–155.
- Poupon, F., Mangin, J.-F., Hasboun, D., Magnin, I., Frouin, V., 1998. Multi-object Deformable Templates Dedicated to the Segmentation of Brain Deep Structures. In: *MICCAI'98, MIT, Lecturer Notes on Computer Science*, vol. 1496. Springer, Berlin, pp. 1134–1143.
- Régis, J., Mangin, J.-F., Frouin, V., Sastre, F., Peragut, J.C., Samson, Y., 1995. Generic model for the localization of the cerebral cortex and preoperative multimodal integration in epilepsy surgery. *Stereotactic and Functional Neurosurgery* 65, 72–80.
- Rivière, D., Mangin, J.-F., Papadopoulos-Orfanos, D., Martinez, J.-M., Frouin, V., Régis, J., 2002. Automatic recognition of cortical sulci of the human brain using a congregation of neural networks. *Medical Image Analysis* 6 (2), 77–92.
- Shen, D., Davatzikos, C., 2003. Very high-resolution morphometry using mass-preserving deformations and hammer elastic registration. *Neuroimage* 18 (1), 28–41.
- Styner, M., Gerig, G., Lieberman, J., Jones, D., Weinberger, D., 2003. Statistical shape analysis of neuroanatomical structures based on medial models. *Medical Image Analysis* 7 (3), 207–220.
- Toga, A.W., Thompson, P.M., 2002. New approaches in brain morphometry. *American Journal of Geriatric Psychiatry* 10 (1), 13–23.
- Van Essen, D.C., 1997. A tension-based theory of morphogenesis and compact wiring in the central nervous system. *Nature* 385, 313–318.
- Venables, W.N., Ripley, B.D., 2002. *Modern Applied Statistics with S*. Springer, Berlin.
- Watkins, K.E., Paus, T., Lerch, J.P., Zijdenbos, A., Collins, D.L., Neelin, P., Taylor, J., Worsley, K.J., Evans, A.C., 2001. Structural asymmetries in the human brain: a voxel-based statistical analysis of 142 mri scans. *Cerebral Cortex* 11 (9), 868–877.
- White, L.E., Lucas, G., Richards, A., Purves, D., 1994. Cerebral asymmetry and handedness. *Nature* 368, 197–198.